Prospective high thermoelectric performance of the heavily *p*-doped half-Heusler compound CoVSn

Hongliang Shi,[1] Wenmei Ming,[2] David S. Parker,[2] Mao-Hua Du,[2] and David J. Singh[3]

[1]*Department of Physics, Key Laboratory of Micro-Nano Measurement-Manipulation and Physics (Ministry of Education), Beihang University, Beijing 100191, China*

[2]*Materials Science and Technology Division, Oak Ridge National Laboratory, Oak Ridge, Tennessee 37831, USA*

[3]*Department of Physics and Astronomy, University of Missouri, Columbia, Missouri 65211-7010, USA*

(Received 17 December 2016; revised manuscript received 17 April 2017; published 11 May 2017)

The electronic structure and transport properties of the half-Heusler compound CoVSn are studied systematically by combining first-principles electronic structure calculations and Boltzmann transport theory. The band structure at the valence-band edge is complex with multiple maxima derived from hybridized transition element *d* states. The result is a calculated thermopower larger than 200 μV/K within a wide range of doping concentrations and temperatures for heavily doped *p*-type CoVSn. The thermoelectric properties additionally benefit from the corrugated shapes of the hole pockets in our calculated isoenergy surfaces. Our calculated power factor $S^2\sigma/\tau$ (with respect to an average unknown scattering time) of CoVSn is comparable to that of FeNbSb. A smaller lattice thermal conductivity can be expected from the smaller group velocities of acoustical modes compared to FeNbSb. Overall, good thermoelectric performance for CoVSn can be expected by considering the electronic transport and lattice thermal conductivity.

DOI: 10.1103/PhysRevB.95.195207

I. INTRODUCTION

Thermoelectric devices can directly convert thermal to electrical energy and have many applications, such as refrigeration and power generation through waste-heat recovery. The performance of a thermoelectric material is characterized by a dimensionless figure of merit ZT by the following expression:

$$ZT = \frac{S^2\sigma T}{\kappa_e + \kappa_l}. \quad (1)$$

Here, S is the Seebeck coefficient or thermopower, σ is the electrical conductivity, T is the absolute temperature, κ_e is the electronic thermal conductivity, and κ_l is the lattice thermal conductivity. The Seebeck coefficient is decreased as the carrier concentration n is increased, whereas σ behaves in the opposite way. Therefore, in order to get the high power factor ($S^2\sigma$), there is a compromise between the large Seebeck coefficient and the high electrical conductivity [1,2]. The electrical conductivity can be expressed by $\sigma = ne\mu$, where n is the carrier concentration and μ is the carrier mobility. Notice that an important factor that affects carrier mobility is the carrier effective mass, which is directly determined by the band-structure properties of thermoelectric materials.

Unlike thermoelectric materials, such as $(Bi,Sb)_2Te_3$ [3,4], Pb(Te,Se) [3,4], and SnSe [5] with band-edge states consisting of *s* and *p* states, there is another class of thermoelectric materials, half-Heusler (HH) alloys, which have flat band-edge states because of the more localized *d* orbitals of transition-metal constituents [6]. The heavy band is not favorable for carrier mobility due to the resulting large effective mass, whereas it is beneficial to thermopower as discussed in Ref. [7]. Half-Heuslers are ternary compounds, ABC (space-group $F\bar{4}3m$), which consist of a late transition metal, an early transition metal, and one main group element, such as group IV or V. Here, we only consider the semiconducting half-Heusler alloys with 18 valence electrons [8].

A large power factor and low thermal conductivity are essential for a high ZT. HH-type thermoelectric materials, such as *n*-type ZrNiSn [9], *p*-type ZrCoSb [10], and *p*-type FeNbSb [11] have attracted particular attention due to their high-temperature stability and good thermoelectric performance resulting from the high power factor at high temperatures [9–15]. A high ZT of 1.5 was reported in the *p*-type $FeNb_{1-x}Hf_xSb$ alloy at 1200 K [12]. The reported power factor ranges from 4.3 to 5.5 $\times 10^{-3}$ W m^{-1} K^{-2} at p_{opt} of $\sim 2 \times 10^{21}$ cm^{-3} at 800 K for $FeNb_{1-x}Hf_xSb$ [12]. This is in contrast to the power factor of only 1.4 $\times 10^{-3}$ W m^{-1} K^{-2} for *p*-type SnSe with ZT of 2.0 around 773 K [5]. It is therefore clear that the drawback of HH thermoelectric materials is their high thermal conductivity. For example, for $FeNb_{0.88}Hf_{0.12}Sb$ at 1200 K, the total thermal conductivity is approximately 4 W m^{-1} K^{-1} [12], whereas for hole-doped SnSe, the total thermal conductivity is about 0.55 W m^{-1} K^{-1} [5]. Therefore, in order to raise the ZT of HH compounds higher, it is important to further optimize the properties of HH compounds of those already studied or find new HH compounds with lower thermal conductivity and/or higher power factors.

In this paper, the electronic properties of the half-Heusler compound CoVSn are studied within density functional theory, followed by its transport properties by Boltzmann transport theory. The phonon dispersions also are studied by lattice dynamics calculation. The group velocities of acoustical branches for several typical half-Heusler thermoelectric materials are calculated. This provides qualitative information regarding the lattice conductivity in relation to CoVSn. We show the potential of CoVSn as a good performance thermoelectric material based on calculated material properties.

II. METHODS

Our electronic structure calculations are performed using the linearized augmented-plane-wave method [16] as implemented in the WIEN2K code [17]. The volume of the half-Heusler compounds studied here is obtained using the Perdew-Burke-Ernzerhof (PBE) generalized-gradient

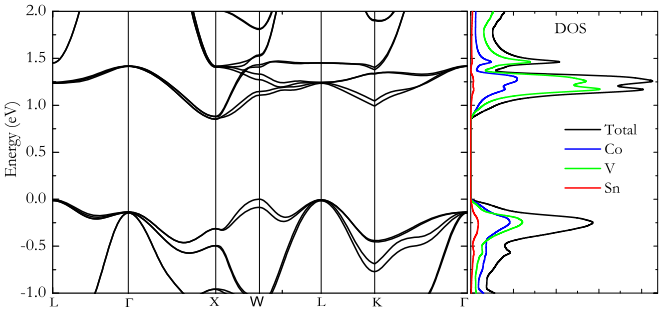

FIG. 1. Calculated band structure together with DOS of CoVSn using the MBJ with SOC. The Fermi level is set to zero.

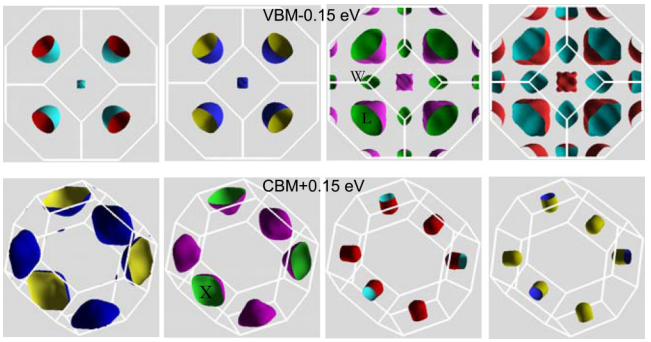

FIG. 2. The calculated isoenergy surfaces for CoVSn near the VBM and CBM. There are four bands across the energy of VBM-0.15 eV as shown in the top panel as CBM + 0.15 eV is shown in the bottom panel. The high-symmetry k points, such as L, W, and X are marked.

approximation [18]. The optimized lattice constant of 5.828 Å for CoVSn is used in all our calculations except for the phonon calculation. The band gap is important for thermoelectric properties. We calculate the electronic structure using the modified Becke-Johnson (MBJ) potential [19]. This potential gives improved band gaps for simple semiconductors and insulators as compared to standard density functionals [19,20]. Our transport coefficients are calculated using Boltzmann theory within the constant scattering time approximation [21] as implemented in the BOLTZTRAP code [22] based on the electronic structure obtained with the MBJ potential. This method has been used successfully to calculate the thermopower of many thermoelectric materials [23,24]. The spin-orbit coupling (SOC) is considered in current electronic structure and transport calculations. Well-converged basis sets defined by a cutoff $RT_{\max} = 9.0$ for the plane-wave vector plus local orbitals for the semicore states are used. Here, $k_{\max}$ is the plane-wave cutoff, and R is the sphere radius. For Co, Sn, and V, the radii are taken as 2.37, 2.37, and 2.31 bohr, respectively. A k-point sampling of $8 \times 8 \times 8$ is used for total energy calculations. A much denser k-point mesh $48 \times 48 \times 48$ is used for transport calculations, and good convergence has been achieved.

III. RESULTS AND DISCUSSION

Our calculated band structure together with the density of states (DOS) for CoVSn using the MBJ potential is shown in Fig. 1. The states close to the valence-band edge mainly are contributed by transition-metal elements Co and V, and further analyses show that there are mainly d orbitals (not shown here) as discussed before. Between the energies 0 and -0.25 eV, the density of states increases very quickly, which will lead to high thermopower. As for the band structure, our calculated band gap (W-X) for CoVSn is 0.85 eV. The valence-band maximum (VBM) is at the W point, which is only slightly higher than the L point for about 6 meV. We also notice that the band maxima at the Γ and X points are only 0.14 and 0.31 eV lower than that of the W point, respectively.

Therefore this compound shows converged bands at the W and L points, which is a feature that has been associated with thermoelectric performance [25]. Furthermore both of these points have degenerate or near-degenerate bands at the maximum, which can lead to additional enhancement of the power factor. It also leads to complex-shaped bands, which is also favorable for thermoelectric performance. These band-structure effects—in particular the band *degeneracy*, complex band shapes, and band *convergence* are critical to the transport properties of this material. The conductivity at the fixed Seebeck coefficient—a key parameter for a useful thermoelectric–is therefore substantially enhanced relative to that of a single isolated parabolic band extremum similar to the certain IV-VI thermoelectric semiconductors with complex electronic structures [26].

The importance of increased band degeneracy also is demonstrated in Bi_2Te_3 [27] and SnSe [5] systems. Further insight also can be obtained from the isoenergy surface of CoVSn as presented in Fig. 2. The four isoenergy surfaces in the top panel of Fig. 2 correspond to four bands across the energy of VBM-0.15 eV. The first two isoenergy surfaces with pockets at the L point are close to ellipsoids, whereas the last two have deviations from spherical or ellipsoidal shapes, particularly the last one with an obvious corrugated shape [26]. We also notice that, at the Γ point, the pocket becomes larger and larger and the shape of the pocket becomes more and more complicated. In the bottom panel of Fig. 2, the four isoenergy surfaces corresponding to four bands across the energy of the conduction-band minimum (CBM) + 0.15 eV are shown. The first two pockets have some deviations from spherical or ellipsoidal shapes, whereas the last two are close to ellipsoids. The thermopower can be enhanced from the deviations of the isoenergy surface from spherical or ellipsoidal shapes, and the greater the deviation, the greater the enhancement [27]. Therefore, the better thermopower of the p-type- than that of the n-type-doped CoVSn can be expected according to our above discussions and will be confirmed by our thermopower calculations in the following.

The doping dependence of the thermopower is shown for various temperatures in Fig. 3. The thermopower is isotropic since the crystal structure of CoVSn is cubic. For the p type, one notes that the thermopower is better than that of the n type as a function of carrier concentration for all temperatures. This originates from the band-structure difference between the bands near the VBM and CBM as depicted in Figs. 1 and 2. Both for n and for p types, for all temperatures, CoVSn displays a wide range of carrier concentration where the thermopower is larger than 200 μV/K. For the p type, at 1000

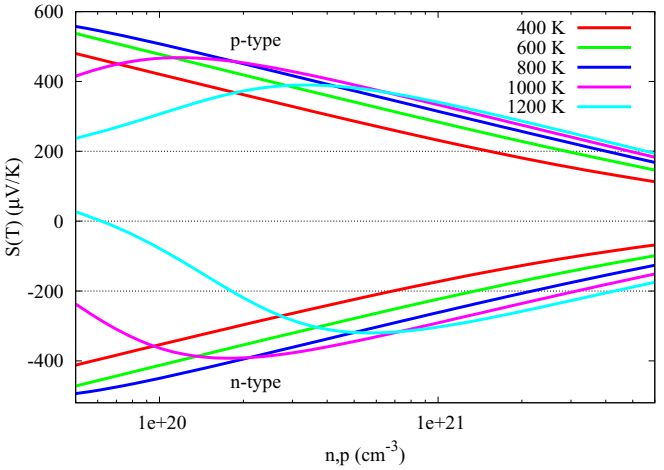

FIG. 3. The calculated Seebeck coefficient as a function of carrier concentration for CoVSn for p-type and n-type doping. The horizontal dashed line indicates a thermopower magnitude of 200 μV/K, generally the minimum necessary for a high-performance thermoelectric.

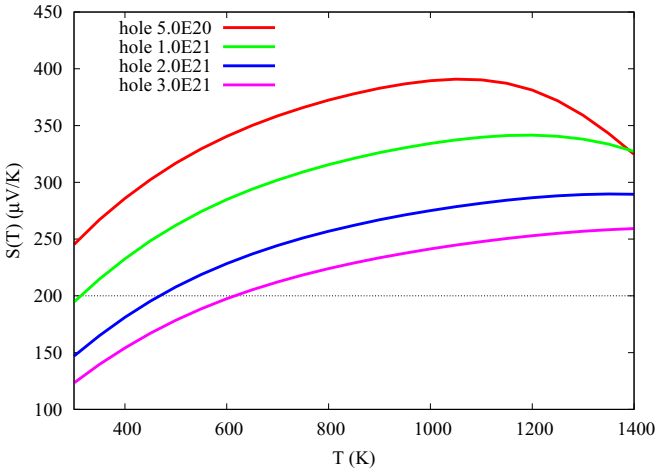

FIG. 4. The calculated thermopower for CoVSn at some fixed concentrations as a function of temperature.

and 1200 K, the highest thermopowers are 470 and 390 μV/K at concentrations of 1.2×10^{20} and 3.3×10^{20} cm^{-3}, respectively. For the n type, at 1000 and 1200 K, the highest thermopowers are -390 and -320 μV/K at concentrations of 1.9×10^{20} and 5.6×10^{20} cm^{-3}, respectively. Notice that at the same temperature, such as 1000 or 1200 K, the highest thermopower for the p type is higher than that of the n type at a relatively lower carrier concentration. Generally, for most materials, optimum performance typically occurs at carrier concentrations above those where the maximum thermopower occurs. As we mentioned before, for half-Heusler alloys, in order to get a high-performance thermoelectric, the optimum carrier concentration is around 10^{21} cm^{-3} [12]. One notes that, at high temperatures of 1000 and 1200 K, up to 4×10^{21} cm^{-3}, the thermopower for CoVSn is still higher than 200 μV/K. There is also a clear bipolar effect for both n and p types at high temperatures where it is well below the optimal carrier concentration regime.

To make the temperature dependence of thermopower more clear, the temperature dependence results at four fixed hole concentrations are presented in Fig. 4. For concentrations of 5.0×10^{20} and 1.0×10^{21} cm^{-3}, the highest thermopowers are about 390 and 340 μV/K at temperatures of 1050 and 1150 K, respectively, whereas for concentrations of 2.0×10^{21} and 3.0×10^{21} cm^{-3}, the thermopowers are approximately 286 and 252 μV/K at 1200 K.

The power factor of $S^2\sigma/\tau$ (with respect to an average unknown scattering time) at 1000, 1100, and 1200 K for p-type doping is shown in Fig. 5. Our calculated power factor of $S^2\sigma/\tau$ for FeNbSb also is plotted for comparison. The plot depicts comparable behavior for FeNbSb and CoVSn with a little smaller for the latter. For example, at 1000 K and 1.0×10^{21}, our calculated $S^2\sigma/\tau$'s for CoVSn and FeNbSb are 10.5 and 13 (in units of 10^{11} W K^{-2} ms^{-1}), respectively.

For a good thermoelectric material, the thermal conductivity, especially the lattice part κ_l, which is determined by the lattice dynamics, must be low. We performed lattice dynamics calculations for CoVSn using the PBE functional [18] for the exchange-correlation potential and the projector augmented-wave method [28] as implemented in the Vienna *ab initio* simulation package [29]. A $2 \times 2 \times 2$ k-point grid in a $3 \times 3 \times 3$ supercell containing 81 atoms is used along with an energy cutoff of 500 eV. The optimized lattice constant is 5.806 Å here for the phonon dispersion calculation. Our calculated phonon dispersion together with the phonon density of states is shown in Fig. 6. There are three acoustical branches and six optical branches since three atoms are in the primitive cell. There is a gap between the acoustical and the optical modes. For the acoustical modes, Sn dominates in the density of states since it is the heaviest element among Co, V, and Sn. Co and V contribute most to the optical modes.

Phonon acoustic branches dominate lattice thermal conductivity since they have greater energy dispersion and therefore a broader distribution of phonon velocities, whereas the optical branches have quite weak energy dispersion, and therefore the velocity is low and make small contributions to lattice thermal conductivity [30]. Since low sound speed is important for a

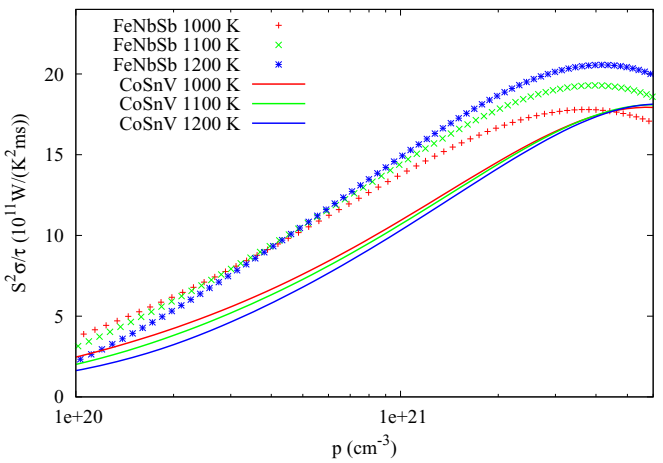

FIG. 5. The calculated power factor of $S^2\sigma/\tau$ for CoVSn and FeNbSb at some fixed temperatures as a function of carrier concentrations.

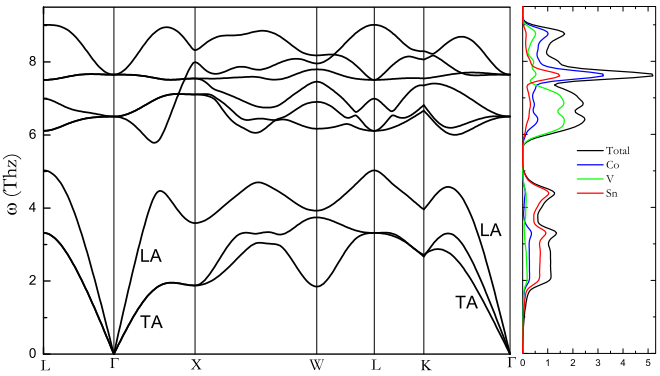

FIG. 6. The calculated phonon dispersion and phonon density of states for CoVSn.

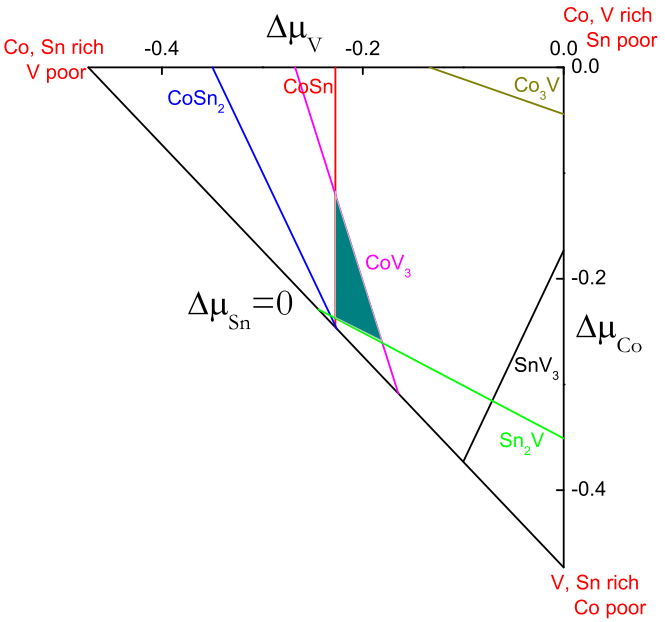

FIG. 7. The calculated phase diagram for CoVSn. The stable region for CoVSn is shaded. The unit for chemical potentials $\Delta\mu_{Co}$ and $\Delta\mu_{V}$ is eV.

reduced κ_l, it is natural to search thermoelectric materials with small slopes of acoustical modes.

In the following, in order to make a comparison with other good half-Heusler thermoelectric alloys, such as FeNbSb, ZrNiSn, and ZrCoSb, the group velocities of the acoustic modes are calculated and collected in Table I, which mainly determines the lattice thermal conductivity. Two directions Γ-X [(001)] and Γ-L [(111)] along with the transverse acoustical (TA) branch and the longitudinal acoustical (LA) branch are considered. Note that TA branches are degenerate in the Γ-X and Γ-L directions. For CoVSn, the TA and LA sound speeds are 2573, 5709, 3136, and 5116 m/s, respectively, along the above two directions. For FeNbSb, its TA and LA sound speeds are 2940, 5997, 3503, and 5361 m/s, respectively, and for ZrCoSb, its TA and LA sound speeds are 2854, 5780, 3365, and 5205 m/s. Therefore, among CoVSn, FeNbSb, and ZrCoSb, CoVSn has the smallest acoustic speeds. Based on our above discussions, compared to FeNbSb and ZrCoSb, the conclusion is that the CoVSn material has good potential for lowering thermal conductivity relative to the other compounds since its sound speeds are smallest. This is in accord with direct lattice thermal conductivity calculations [31]. Note that Bi_2Te_3 has smaller lattice thermal conductivity, which is consistent with its corresponding smaller sound speeds, compared to the above half-Heusler alloys. For Bi_2Te_3, along the Γ-L direction, the sound speeds of TA and LA are 1395, 1728, and 2394 m/s, respectively, and along the Γ-Z direction, the speeds are 1774 and 1811 m/s [27].

TABLE I. Calculated group velocities of acoustical modes along the Γ-X and Γ-L directions. The unit is m/s.

	Γ to X		Γ to L	
	TA	LA	TA	LA
CoVSn	2573	5709	3136	5116
CoSnNb	2847	5813	3330	5277
IrGeNb	3002	4991	2722	5251
FeNbSb	2940	5997	3503	5361
ZrCoSb	2854	5780	3365	5205
ZrNiSn	2868	5516	3150	5200

Experimentally, Lue *et al.* [32] have shown that CoVSn can be produced, at least, with partial atomic ordering on the half-Heusler lattice. They successfully prepared CoVSn in a rf induction furnace from elemental ingredients, whereas attempts by the arc-melting method were not successful [32]. Another study of $Ti_{1-x}V_xCoSb_{1-x}Sn_x$ found that x cannot be increased beyond 0.4, which indicates that CoVSn cannot be synthesized by a conventional solid-state reaction [33]. Theoretically Carrete *et al.* predicted CoVSn is both thermally and mechanically stable [31], whereas Zakutayev *et al.* predict CoVSn is not stable theoretically [34], based on calculations using the fitted elemental-phase reference energies method [35]. In a very recent work, Ma *et al.* [36] reported that almost all the experimentally synthesized half-Heusler compounds lie on or close to the convex hull with hull distances between 0.0 and about 0.1 eV/atom. They selected 110 compounds (experimentally reported and unreported) in which they find that (shown in Fig. 6 of Ref. [36]) that the vast majority of the reported half-Heusler compounds that have been synthesized experimentally lie on or close to the calculated convex hull-37 compounds are on the convex hull (i.e., a hull distance of 0 eV/atom) and an additional 52 lie relatively close to it (i.e., a hull distance less than about 0.1 eV/atom) [36]. They predicted that CoVSn is in the half-Heusler structure because its hull distance is only 0.012 eV/atom just above the convex hull [36]. We also performed stability calculations considering competing phases. Our total energy calculations for the competing phases show that CoVSn is thermodynamically stable with the PBE functional, which is shown in the shaded region in Fig. 7. With careful control of growth conditions (which affects the elemental chemical potentials $\Delta\mu$), the synthesis of the single-phase CoVSn is possible. According to the above discussions, the method and condition that were used in the synthesis of

CoVSn should be controlled carefully. In any case it may be that CoVSn can be synthesized by nonequilibrium ways, e.g., quenching via melt spinning or in thin-film deposition. Melt spinning is a method that was used for other nanostructured thermoelectrics [37,38].

IV. SUMMARY

The electronic structure and potential thermoelectric performance of the half-Heusler alloy CoVSn are investigated theoretically. A high thermopower is obtained for CoVSn, particularly for the p-type doping. This originates from several close valence-band maxima and corrugated shapes in the isoenergy surface according to our calculations. This type of complex band shape and degeneracy enables resolution of the conundrum posed by normally contradictory requirements of high thermopower and high conductivity needed to obtain high ZT. Our calculated power factor of $S^2\sigma/\tau$ for CoVSn can be comparable to that of FeNbSb at the optimal carrier concentration. A smaller group velocity of acoustical modes for CoVSn indicates that the possibility of smaller lattice thermal conductivity exists, which also is good for the overall thermoelectric performance.

ACKNOWLEDGMENTS

H.S. was supported by the National Natural Science Foundation of China (NSFC) under Grant No. 11604007 and the start-up funding at Beihang University. Work at the University of Missouri was supported by the Department of Energy through the S3TEC EFRC, Award No. DE-SC0001299/DE-FG02-09ER46577. The work at ORNL (W.M., D.S.P., and M.-H.D.) was supported by the U.S. Department of Energy, Office of Science, Basic Energy Sciences, Materials Sciences and Engineering Division.

[1] C. Wood, Materials for thermoelectric energy conversion, Rep. Prog. Phys. **51**, 459 (1988).
[2] J. Yang, L. Xi, W. Qiu, L. Wu, X. Shi, L. Chen, J. Yang, W. Zhang, C. Uher, and D. J. Singh, On the tuning of electrical and thermal transport in thermoelectrics: An integrated theory-experiment perspective, npj Comput. Mater. **2**, 15015 (2016).
[3] A. F. Ioffe, *Semiconductor Thermoelements and Thermoelectric Cooling* (Inforsearch, London, 1957).
[4] D. M. Rowe, *CRC Handbook of Thermoelectrics* (CRC, New York, 1995).
[5] L. D. Zhao, G. J. Tan, S. Q. Hao, J. Q. He, Y. L. Pei, H. Chi, H. Wang, S. K. Gong, H. B. Xu, V. P. Dravid, C. Uher, G. J. Snyder, C. Wolverton, and M. G. Kanatzidis, Ultrahigh power factor and thermoelectric performance in hole-doped single-crystal SnSe, Science **351**, 141 (2016).
[6] C. Uher, J. Yang, S. Hu, D. T. Morelli, and G. P. Meisner, Transport properties of pure and doped MNiSn (M = Zr, Hf), Phys. Rev. B **59**, 8615 (1999).
[7] K. Kuroki and R. Arita, Pudding mold band drives large thermopower in Na_xCoO_2, J. Phys. Soc. Jpn. **76**, 083707 (2007).
[8] D. Jung, H.-J. Koo, and M.-H. Whangbo, Study of the 18-electron band gap and ferromagnetism in semi-Heusler compounds by non-spin-polarized electronic band structure calculations, J. Mol. Struct.: THEOCHEM **527**, 113 (2000).
[9] C. Yu, T.-J. Zhu, R.-Z. Shi, Y. Zhang, X.-B. Zhao, and J. He, High-performance half-Heusler thermoelectric materials $Hf_{1-x}Zr_xNiSn_{1-y}Sb_y$ prepared by levitation melting and spark plasma sintering, Acta Mater. **57**, 2757 (2009).
[10] S. R. Culp, J. W. Simonson, S. J. Poon, V. Ponnambalam, J. Edwards, and T. M. Tritt, (Zr, Hf)Co(Sb, Sn) half-Heusler phases as high-temperature (>700 °C) p-type thermoelectric materials, Appl. Phys. Lett. **93**, 022105 (2008).
[11] C. Fu, T. Zhu, Y. Liu, H. Xie, and X. Zhao, Band engineering of high performance p-type FeNbSb based half-Heusler thermoelectric materials for figure of merit zT > 1, Energy Environ. Sci. **8**, 216 (2015).
[12] C. Fu, S. Bai, Y. Liu, Y. Tang, L. Chen, X. Zhao, and T. Zhu, Realizing high figure of merit in heavy-band p-type half-Heusler thermoelectric materials, Nat. Commun. **6**, 8144 (2015).
[13] L. Chen, S. Gao, X. Zeng, A. M. Dehkordi, T. M. Tritt, and S. J. Poon, Uncovering high thermoelectric figure of merit in (Hf, Zr)NiSn half-Heusler alloys, Appl. Phys. Lett. **107**, 041902 (2015).
[14] R. He, L. Huang, Y. Wang, G. Samsonidze, B. Kozinsky, Q. Zhang, and Z. Ren, Enhanced thermoelectric properties of n-type NbCoSn half-Heusler by improving phase purity, APL Mater. **4**, 104804 (2016).
[15] G. Fiedler and P. Kratzer, Ternary semiconductors NiZrSn and CoZrBi with half-Heusler structure: A first-principles study, Phys. Rev. B **94**, 075203 (2016).
[16] *Planewaves, Pseudopotentials, and the LAPW Method*, second ed., edited by D. J. Singh and L. Nordstrom (Springer, Berlin, 2006).
[17] P. Blaha, K. Schwarz, G. Madsen, D. Kvasnicka, and J. Luitz, WIEN2K, *An Augmented Plane Wave + Local Orbitals Program for Calculating Crystal Properties* (K. Schwarz, Technical University Wien, Austria, 2001).
[18] J. P. Perdew, K. Burke, and M. Ernzerhof, Generalized Gradient Approximation Made Simple, Phys. Rev. Lett. **77**, 3865 (1996).
[19] F. Tran and P. Blaha, Accurate Band Gaps of Semiconductors and Insulators with a Semilocal Exchange-Correlation Potential, Phys. Rev. Lett. **102**, 226401 (2009).
[20] D. Koller, F. Tran, and P. Blaha, Merits and limits of the modified Becke-Johnson exchange potential, Phys. Rev. B **83**, 195134 (2011).
[21] D. Parker and D. J. Singh, High-temperature thermoelectric performance of heavily doped PbSe, Phys. Rev. B **82**, 035204 (2010).
[22] G. K. H. Madsen and D. J. Singh, Boltztrap. A code for calculating band-structure dependent quantities, Comput. Phys. Commun. **175**, 67 (2006).
[23] D. J. Singh, Electronic and thermoelectric properties of $CuCoO_2$: Density functional calculations, Phys. Rev. B **76**, 085110 (2007).
[24] D. Parker and D. J. Singh, Potential Thermoelectric Performance from Optimization of Hole-Doped Bi_2Se_3, Phys. Rev. X **1**, 021005 (2011).

[25] Y. Pei, X. Shi, A. LaLonde, H. Wang, L. Chen, and G. J. Snyder, Convergence of electronic bands for high performance bulk thermoelectrics, Nature (London) **473**, 66 (2011).

[26] X. Chen, D. Parker, and D. J. Singh, Importance of non-parabolic band effects in the thermoelectric properties of semiconductors, Sci. Rep. **3**, 3168 (2013).

[27] H. Shi, D. Parker, M.-H. Du, and D. J. Singh, Connecting Thermoelectric Performance and Topological-Insulator Behavior: Bi_2Te_3 and Bi_2Te_2Se from First Principles, Phys. Rev. Appl. **3**, 014004 (2015).

[28] G. Kresse and D. Joubert, From ultrasoft pseudopotentials to the projector augmented-wave method, Phys. Rev. B **59**, 1758 (1999).

[29] G. Kresse and J. Furthmuller, Efficient iterative schemes for ab *initio* total-energy calculations using a plane-wave basis set, Phys. Rev. B **54**, 11169 (1996).

[30] P. Pichanusakorn and P. Bandaru, Nanostructured thermoelectrics, Mater. Sci. Eng., R **67**, 19 (2010).

[31] J. Carrete, W. Li, N. Mingo, S. Wang, and S. Curtarolo, Finding Unprecedentedly Low-Thermal-Conductivity Half-Heusler Semiconductors via High-Throughput Materials Modeling, Phys. Rev. X **4**, 011019 (2014).

[32] C. S. Lue, Y. Oner, D. G. Naugle, and J. H. Ross, Magnetism of new semi-Heusler compounds FeVSn and CoVSn, IEEE Trans. Magn. **37**, 2138 (2001).

[33] M. Asaad, J. Buckman, R. I. Smithc, and J. W. G. Bos, Thermoelectric properties and high-temperature stability of the $Ti_{1-x}V_xCoSb_{1-x}Sn_x$ half-Heusler alloys, RSC Adv. **6**, 56511 (2016).

[34] A. Zakutayev, X. Zhang, A. Nagaraja, L. Yu, S. Lany, T. Mason, D. S. Ginley, and A. Zunger, Theoretical prediction and experimental realization of new stable inorganic materials using the inverse design approach, J. Am. Chem. Soc. **135**, 10048 (2013).

[35] V. Stevanović, S. Lany, X. Zhang, and A. Zunger, Correcting density functional theory for accurate predictions of compound enthalpies of formation: Fitted elemental-phase reference energies, Phys. Rev. B **85**, 115104 (2012).

[36] J. Ma, V. I. Hegde, K. Munira, Y. Xie, S. Keshavarz, D. T. Mildebrath, C. Wolverton, A. W. Ghosh, and W. H. Butler, Computational investigation of half-Heusler compounds for spintronics applications, Phys. Rev. B **95**, 024411 (2017).

[37] W. Xie, X. Tang, Y. Yan, Q. Zhang, and T. Tritt, Unique nanostructures and enhanced thermoelectric performance of melt-spun BiSbTe alloys, Appl. Phys. Lett. **94**, 102111 (2009).

[38] G. Tan, W. Liu, S. Wang, Y. Yan, H. Li, X. Tang, and C. Uher, Rapid preparation of $CeFe_4Sb_{12}$ skutterudite by melt spinning: Rich nanostructures and high thermoelectric performance, J. Mater. Chem. A **1**, 12657 (2013).